Effects of lithium intercalation in bilayer graphene

Xi Wu,[1] Fawei Zheng,[2,3] Feiyu Kang,[1,*] and Jia Li[1,†]

[1]*Shenzhen Geim Graphene Center and Institute of Materials Research, Shenzhen International Graduate School, Tsinghua University, Shenzhen 518055, China*

[2]*Centre for Quantum Physics, Key Laboratory of Advanced Optoelectronic Quantum Architecture and Measurement (MOE), School of Physics, Beijing Institute of Technology, Beijing 100081, China*

[3]*Beijing Key Lab of Nanophotonics and Ultrafine Optoelectronic Systems, School of Physics, Beijing Institute of Technology, Beijing 100081, China*

(Received 11 July 2022; revised 3 February 2023; accepted 3 April 2023; published 11 April 2023)

Modulation of the Dirac cone of graphene has been highly desired to enrich the exotic properties of graphene. Intercalation of Li into multilayer graphene could lead to the gap opening of the Dirac cone of graphene. Here, using density functional theory calculations, we identify the stable intercalated structure and the corresponding evolution of band structures in the intercalation process of Li into bilayer graphene (BLG). The generalized Kekulé order beyond the traditional $\sqrt{3} \times \sqrt{3}$ supercell has been observed to modulate the Dirac cones of BLG by opening a gap or splitting the electron and hole pocket, contributed by the Kekulé-O and the Kekulé-Y distortion, respectively. Our work provides a further understanding of the modulation of the Dirac cone of graphene and can serve as a landmark for experiment to investigate the Li-intercalated BLG.

DOI: 10.1103/PhysRevB.107.165409

I. INTRODUCTION

Graphene, the first observed two-dimensional material with two sublattices in its hexagonal lattice, has Dirac cones with linear energy dispersion located at the K and K' points of its Brillouin zone, which are protected by inversion and time-reversal symmetry [1–3]. The gapless Dirac cones in graphene can be opened by applying different potentials to two sublattices [4–6] or by introducing the intervalley coupling between Dirac cones at the K and K' points [7–9]. The Bernal stacking bilayer graphene (BLG) can be regarded as an example of the gap opening in the hexagonal lattice with two sublattices in different potential energies and one Dirac cone of BLG at the K point is opened [10]. In addition, the gap opening of the Dirac cone in graphene caused by the intervalley coupling can be realized by forming a specific type of Kekulé distortion, which can be induced by applying an external superlattice potential [11,12] or by introducing dilute adatoms or defects on graphene [13–15]. In addition, the intercalation of alkali metal is also an effective way to realize the gap opening of the Dirac cone [16,17].

Intercalation of alkali metal into graphite or multilayer graphene is the most classic charge storage mechanism in rechargeable battery technologies [18–20], and the LiC_6 with a superlattice of $(\sqrt{3} \times \sqrt{3})R30^\circ$ and the KC_8 with a superlattice of 2×2 have been regarded as the saturated Li-intercalated and K-intercalated structures, respectively [21–24]. Some exotic properties like superconductivity can also be observed in the saturated Li-intercalated structure of LiC_6 or the Cs-intercalated structure of CsC_6 [25,26]. For the graphene with a superlattice of $(\sqrt{3} \times \sqrt{3})R30^\circ$, the different bond distortion can lead to the Kekulé-Y order with "Y"-shaped bond modulation or to the Kekulé-O order with "O"-shaped bond modulation [27–31]. The Kekulé-Y ordered graphene, realized by a heterostructure of graphene grown on Cu substrate, remains gapless [15,29], while the Kekulé-O ordered graphene has been experimentally evidenced in the saturated Li-intercalated BLG with a superlattice of $(\sqrt{3} \times \sqrt{3})R30^\circ$ [30,31]. However, the stable intercalated structure and the evolution of the band structure during the intercalation of Li into the BLG still need to be further investigated. Here, we report the existence of a generalized Kekulé order beyond the $\sqrt{3} \times \sqrt{3}$ supercell in the intercalation process of Li into BLG. Moreover, by monitoring the corresponding evolution of band structures, we find the modulation of the Dirac cones of the BLG by opening a gap or splitting the electron and hole pocket, which are contributed to the Kekulé-O and the Kekulé-Y distortion, respectively. Our results provide further insights for understanding the underlying mechanism of the band structure of the BLG with the generalized Kekulé order.

II. COMPUTATIONAL METHODS

In this work, density functional theory (DFT) calculations were carried out using the Vienna *ab initio* simulation package (VASP) [32]. The electron-ion interaction and exchange-correlation energy were described by the projector augmented wave potential [33,34] and generalized gradient approximation with the Perdew-Burke-Ernzerhof functional [35], respectively. The van der Waals interaction was described by the DFT-D3 empirical correction [36]. A vacuum space larger than 15 Å was added above the bilayer graphene to eliminate

*fykang@sz.tsinghua.edu.cn
†li.jia@sz.tsinghua.edu.cn

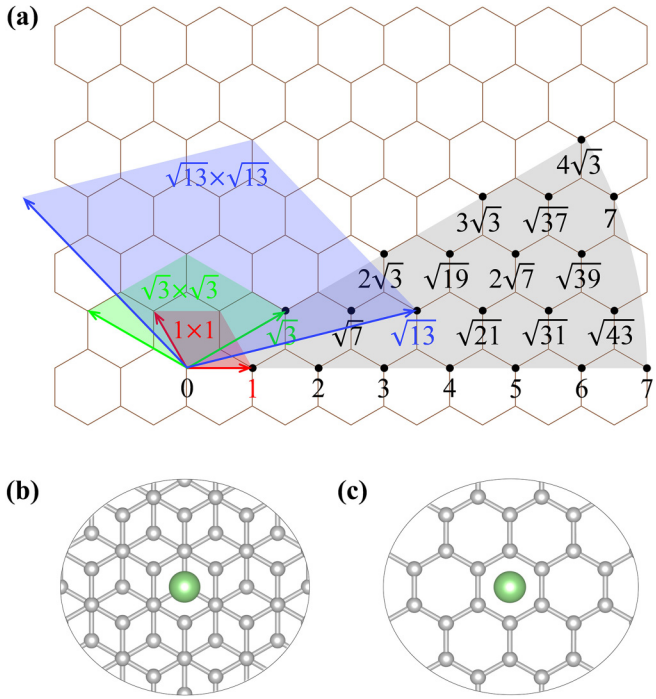

FIG. 1. (a) Schematics of the superlattice of BLG used in the simulation. (b),(c) Top view of AB-stacking and AA-stacking BLG intercalated with Li.

the interaction between the periodically repeated images. The density of the Γ-centered k-point mesh was set as 0.04/Å and 0.02/Å for structure optimization and electronic structure calculation, respectively. The energy cutoff was set to 400 eV, and the energy convergence criterion was set to 10^{-5} eV. All atoms were fully relaxed until the force on each atom was less than 10^{-2} eV/Å. In order to compare the Dirac cones of the bilayer graphene with different concentrations of intercalated Li, the band structures for the supercell of bilayer graphene were unfolded into the Brillouin zone of the primitive cell by the effective band structure method [37].

III. RESULTS AND DISCUSSION

The previous experimental result [38] proposed that the distribution of Li in the intercalated BLG is uniform, especially for the BLG with concentrated Li [39]. The charge transfer from Li to graphene would induce long-range Coulomb repulsion between the positively charged Li, ensuring the hexagonal-ordered state of Li within BLG. Therefore, the whole intercalation process of Li is theoretically investigated from the dilute concentration ($Li_{0.061}C_{12}$) to the extremely high concentration (Li_3C_{12}) by intercalating one Li into different supercells of BLG, as shown in Fig. 1(a). Meanwhile, AA- and AB-stacking orders of BLG are both considered for Li intercalation. After intercalation, Li prefers to locate at the top site of one layer but the hollow site of the other layer of AB-stacking BLG [shown in Fig. 1(b)], while Li prefers to locate at the hollow site of both layers of AA-stacking BLG [shown in Fig. 1(c)].

To estimate the energetic stability of Li in BLG, we firstly determined the intercalation energy (E_i) per Li atom with different concentrations, as shown in Supplemental Material Fig. S1 [40]. It is observed that, as more Li is intercalated into the BLG, E_i would increase, and the Bernal-stacking BLG would transfer from AB- to AA-stacking order. Specifically, the E_i of LiC_{12} (one Li atom intercalated into the $\sqrt{3} \times \sqrt{3}$ supercell of BLG with AA-stacking order, denoted as $\sqrt{3} \times \sqrt{3}$, AA) is −2.04 eV, which is slightly lower than the cohesive energy of Li metal (−1.99 eV). If more Li atoms are intercalated into LiC_{12}, E_i would be higher than the cohesive energy of Li metal, indicating the possibility of Li aggregation. Therefore, LiC_{12} can be considered as the BLG with the saturated concentration of Li. To determine the thermodynamically stable structures of BLG with different concentrations of Li, the convex hulls of BLG during Li intercalation were constructed by calculating the formation energy per Li (E_f), which is defined as

$$E_f = E_{\text{tot}} - E_{\text{sub}} - u_{\text{Li}}, \tag{1}$$

where E_{tot} is the total energy of the BLG supercell with one intercalated Li, E_{sub} is the energy of the BLG supercell, $E_{\text{tot}} - E_{\text{sub}}$ refers to the energy difference between the BLG supercell with and without one intercalated Li, and u_{Li} refers to the chemical potential of Li determined as the energy difference between the AA-stacking BLG with the saturated concentration of Li (Li_xC_{12}) and the pristine AB-stacking BLG without Li intercalation ($u_{\text{Li}} = E_{\text{LiC}_{12}} - E_{\text{C}_{12}}$). As shown in Fig. 2(a), under the dilute concentration of Li (Li_xC_{12}, $0 \leqslant x \leqslant 0.16$), the BLG with AB-stacking order is more stable than that with AA-stacking order. Nevertheless, the stable stacking order of BLG would transform to the AA stacking under the high concentration of Li (Li_xC_{12}, $0.18 \leqslant x \leqslant 1$). The stacking transformation from AB- to AA-stacking order has been elucidated by the variation trend of the intensity ratios between the {0110} peak and the {1210} peak in the selected-area electron diffraction patterns during Li intercalation in BLG [38]. Additionally, besides pristine BLG and LiC_{12} ($\sqrt{3} \times \sqrt{3}$, AA) with the saturated concentration of Li, four Li-intercalated BLG structures of $Li_{0.083}C_{12}$ (6×6, AB), $Li_{0.188}C_{12}$ (4×4, AA), $Li_{0.231}C_{12}$ ($\sqrt{13} \times \sqrt{13}$, AA), and $Li_{0.75}C_{12}$ (2×2, AA) are predicted to be stable, which could be observed in the experiment.

To further investigate the intercalation process of Li into BLG, we provide information on the band structures of stable structures during Li intercalation. For clarity, all band structures shown in this work are the local amplification of Dirac cones, which are completely contributed by the carbon atoms of BLG (shown in Fig. S2 [40]). As shown in Fig. 2(b), the pristine AB-stacking BLG has one pair of π and π^* states degenerating at the K point to form a gapless Dirac cone, and another pair of π and π^* bands is split by the A-B interlayer coupling [10]. With the intercalation of Li, the Fermi level would shift up to the electron pocket of the BLG, indicating electrons would transfer from the Li to the BLG. For $Li_{0.083}C_{12}$ (6×6, AB), there also exists a tiny band splitting of the electron pocket of the Dirac cone. For $Li_{0.188}C_{12}$ (4×4, AA), the stable stacking order would transfer from AB to AA, and the two gapless Dirac cones are located at the K point, where the energies of two Dirac points are all below the Fermi level. It is thus that the number of gapless Dirac cones can be viewed as the indicator of the stacking order of BLG in

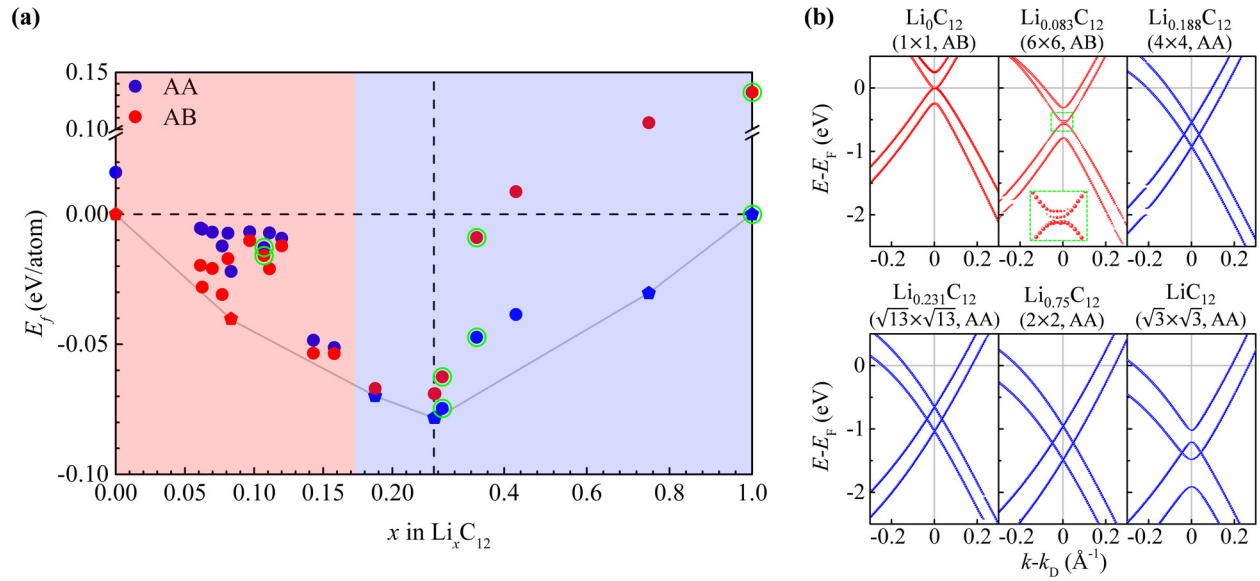

FIG. 2. (a) Formation energy (E_f) convex hull construction for Li-intercalated BLG with different concentrations of Li. In the light-red (light-blue) area, the stable BLG after Li intercalation is AB stacking (AA stacking). Pentagons represent the six stable Li-intercalated BLG structures. Green circles represent the Li-intercalated BLG structures with the generalized Kekulé order. (b) Band structures of six stable Li-intercalated BLG structures.

experiments. For $Li_{0.231}C_{12}$ ($\sqrt{13}\times\sqrt{13}$, AA) and $Li_{0.75}C_{12}$ (2×2, AA), two gapless Dirac cones are preserved while the Fermi level is shifted up due to more electrons transferred from Li to BLG. For LiC_{12} ($\sqrt{3}\times\sqrt{3}$, AA), two obvious gap-opening Dirac cones at the K point are induced by the Kekulé order of Li in the intercalated BLG.

Generally, the gap opening of the Dirac cone caused by Kekulé distortion is inherent in the $\sqrt{3}\times\sqrt{3}$ supercell of graphene. However, the modulation of the Dirac cone might also be observed in other Li-intercalated structures. Here, systematic calculations are performed to investigate the band structures of BLG with different stacking orders and different concentrations of Li. Interestingly, the distinctive modulation of Dirac cones has been observed in other regular BLG supercells. As shown in Fig. 3(a), the obvious band splitting of the electron and hole pocket can be found in AB-stacking BLG with specific intercalation configuration as one Li in $\sqrt{3}\times\sqrt{3}$, 3×3, $2\sqrt{3}\times2\sqrt{3}$, and $3\sqrt{3}\times3\sqrt{3}$ supercells of BLG. However, there is no obvious band splitting of the Dirac cone in other Li-intercalated BLGs with AB-stacking order, as shown in Fig. S3 [40]. Moreover, inequivalent electrons transferred from Li to two individual layers of BLG can induce the internal electric field, which leads to the gap opening of the Dirac cone in the generalized Li-intercalated AB-stacking BLG. However, the gap opening can be occasionally compensated by the band splitting of the electron and hole pocket, resulting in the gaplessness of the Dirac cone in LiC_{12} ($\sqrt{3}\times\sqrt{3}$, AB) and $Li_{0.111}C_{12}$ ($3\sqrt{3}\times3\sqrt{3}$, AA) shown in Fig. 3(a). In comparison, two Dirac cones are both gapped in four Li-intercalated BLGs with AA stacking: LiC_{12} ($\sqrt{3}\times\sqrt{3}$, AA), $Li_{0.333}C_{12}$ (3×3, AA), $Li_{0.25}C_{12}$ ($2\sqrt{3}\times2\sqrt{3}$, AA), and $Li_{0.111}C_{12}$ ($3\sqrt{3}\times3\sqrt{3}$, AA), shown in Fig. 3(b). Therefore, a generalized Kekulé order with the lattice of an integral multiple of $\sqrt{3}$ or 3, which are beyond the traditional $\sqrt{3}\times\sqrt{3}$ supercell, can effectively modulate the Dirac cone of graphene. Nevertheless, for the generalized Kekulé order, there are significant differences between Dirac cones of BLG with different stacking orders. For AA-stacking BLG, the Li are all located at the hollow site, resulting in the formation of the Kekulé-O type pattern for two individual graphene layers. Therefore, the gap opening of two Dirac

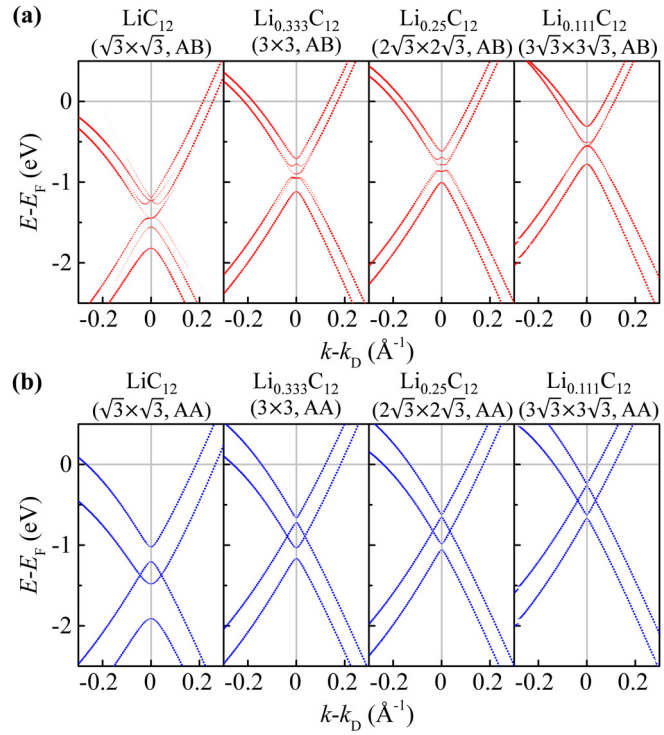

FIG. 3. (a) Band structure of the generalized Kekulé patterned BLG with AB-stacking order. (b) Band structure of the generalized Kekulé patterned BLG with AA-stacking order.

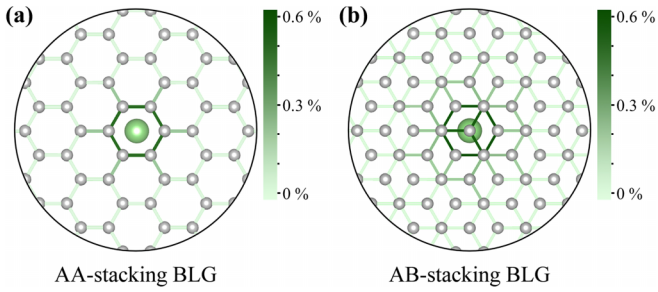

FIG. 4. Illustration of C-C bond stretching in (a) AA-stacking and (b) AB-stacking Li-intercalated BLG with the supercell of $3\sqrt{3} \times 3\sqrt{3}$.

cones can be observed. Whereas for AB-stacking BLG, the Li are located at the top site of one graphene layer and the hollow site of another layer, so there should be a mixture of the Kekulé-O and Kekulé-Y type patterns; and the Kekulé-Y distortion is responsible for the band splitting of the electron and hole pocket of the Dirac cone. However, although some Li-intercalated structures with the generalized Kekulé order may not be the most stable structures, they are metastable structures that may be synthesized by controlling the concentration of Li.

In addition, the length of nonequivalent C-C bonds around the intercalated Li for different BLG supercells are summarized to elucidate the effect of intercalated Li. As shown in Fig. S4 [40], for AA-stacking bilayer graphene, only C-C bonds in one graphene layer are summarized due to the mirror symmetry between the upper and lower graphene layers. However, for the AB-stacking bilayer graphene, the C-C bonds in the upper and lower graphene layers are all summarized since the Li locates at the hollow and top sites of the upper and lower graphene layers, respectively. The selected C-C bond lengths are summarized in Supplemental Material Table S1 [40]. At the beginning of Li intercalation, the nearest-neighbor and next-neighbor C-C bonds closed to the intercalated Li are stretched by about 0.5% and 0.2%, respectively, with respect to the pristine BLG, while other C-C bonds have negligible distortion, as shown in Fig. 4. It is worth noting that the bond stretching would be weakened as the intercalated Li approaches the saturation concentration, and even become negligible when the Li reaches the saturation concentration to form LiC_{12}, in which all C-C bonds have the same length when the Li is located at the hollow sites of the graphene layer. Therefore, the C-C bond distortion of graphene caused by the Li intercalation is not the determining factor to the distinctive modulation of Dirac cones of bilayer graphene with the generalized Kekulé order.

To figure out the origin of the generalized Kekulé order as well as the difference between the Dirac cone introduced by the Kekulé-Y and Kekulé-O distortions, we investigate the characteristics of the Dirac cone of the monolayer graphene caused by the adsorption of Li with the generalized Kekulé order, as shown in Fig. S5 [40]. The Kekulé-O and Kekulé-Y distortions are constructed through the adsorption of Li at the hollow and top sites of graphene, respectively. A distinct change of the Dirac cone has also been observed in monolayer graphene with the lattice of an integral multiple of $\sqrt{3}$ or 3. Interestingly, the Dirac cone of LiC_6 with the Kekulé-O distortion is comparable to the angle-resolved photoemission spectroscopy (ARPES) results [30]. For graphene, the coupling between the valleys at K and K' of the primary cell is vital to the distinctive modulation of the Dirac cone, especially for the gap opening of the Dirac cone caused by the Kekulé distortion in the $\sqrt{3} \times \sqrt{3}$ supercell of graphene. As shown in Fig. 5(a), the Brillouin zone (BZ) of graphene in the primary cell and the supercell of $\sqrt{3} \times \sqrt{3}$ are marked as blue and red hexagons, respectively. The K and K' valley points of the primary cell are located at the six corners of the blue hexagon and the center of the red hexagon that represents the Γ point of the $\sqrt{3} \times \sqrt{3}$ supercell. Once the Kekulé distortion ($\sqrt{3} \times \sqrt{3}$ supercell) is formed, the K and K' valley points of the primary cell will be folded to the Γ point of the $\sqrt{3} \times \sqrt{3}$ supercell. Such a folding of the BZ will induce the intervalley coupling of graphene, leading to the gap opening of the Dirac cone. Similarly, the two valley points K and K' in the BZ of the primary cell can also be folded into the Γ point in the BZ of the 3×3 supercell, shown in Fig. 5(b), indicating the intervalley coupling could also occur in the 3×3 graphene supercell. Therefore, the distortion in a supercell of an integral multiple of $\sqrt{3}$ or 3 can lead to the intervalley coupling since the valley points K and K' of the primary cell can be folded to the Γ point of the supercells. The above distortion can be considered as the generalized Kekulé distortion. The generalized Kekulé distortion would lead to distinctive modulation of the Dirac cone of graphene, while it is also determined by the type of Kekulé distortion, Kekulé-O or Kekulé-Y.

Besides the generalized Kekulé order, the different effects induced by the Kekulé-Y and Kekulé-O distortions on the Dirac cone of graphene have also been observed in the result. As shown in Figs. 5(c) and 5(d), the Kekulé-Y and Kekulé-O distortions lead to the band splitting and the gap opening of the Dirac cone, respectively. Here, the Hamiltonian with four degenerate states at Fermi energy consists of two states induced by two sublattices ($|A\rangle$, $|B\rangle$) at the K point and two states ($|A'\rangle$, $|B'\rangle$) at the K' point. Four degenerate states at Fermi level can be written as

$$|A\rangle = \frac{1}{\sqrt{N}} \sum_{\mathbf{R}_A} e^{i\mathbf{K}\cdot\mathbf{R}_A} |A_{\mathbf{R}}\rangle = \frac{1}{\sqrt{N}} \sum_{m,n} e^{(2\pi i/3)(m+2n)} |A_{m,n}\rangle, \tag{2}$$

$$|B\rangle = \frac{1}{\sqrt{N}} \sum_{\mathbf{R}_B} e^{i\mathbf{K}\cdot\mathbf{R}_B} |B_{\mathbf{R}}\rangle = \frac{1}{\sqrt{N}} \sum_{m,n} e^{(2\pi i/3)(m+2n-1)} |B_{m,n}\rangle, \tag{3}$$

$$|A'\rangle = \frac{1}{\sqrt{N}} \sum_{\mathbf{R}_A} e^{i\mathbf{K}'\cdot\mathbf{R}_A} |A_{\mathbf{R}}\rangle = \frac{1}{\sqrt{N}} \sum_{m,n} e^{(2\pi i/3)(2m+n)} |A_{m,n}\rangle, \tag{4}$$

$$|B'\rangle = \frac{1}{\sqrt{N}} \sum_{\mathbf{R}_B} e^{i\mathbf{K}'\cdot\mathbf{R}_B} |B_{\mathbf{R}}\rangle = \frac{1}{\sqrt{N}} \sum_{m,n} e^{(2\pi i/3)(2m+n-1)} |B_{m,n}\rangle, \tag{5}$$

where $\mathbf{R}_A = m(\mathbf{a} - \mathbf{c}) + n(\mathbf{b} - \mathbf{c}) + \mathbf{r}_A$ and $\mathbf{R}_B = m(\mathbf{a} - \mathbf{c}) + n(\mathbf{b} - \mathbf{c}) + \mathbf{r}_B$ are the positions of carbon atoms in sublattices A and B, respectively. $\mathbf{r}_A$ and $\mathbf{r}_B$ are the positions

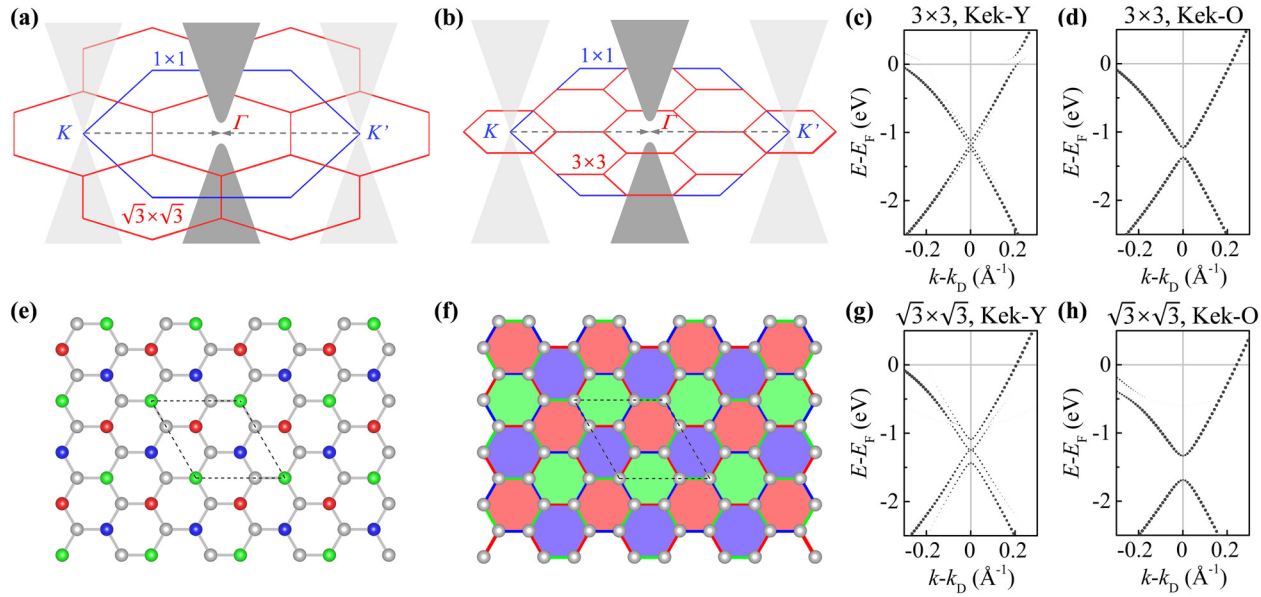

FIG. 5. (a),(b) Schematics of the intervalley coupling at the Γ point of graphene with $\sqrt{3} \times \sqrt{3}$ and 3×3 supercells. (c),(d) Band structure of the 3×3 graphene lattice with the Kekulé-Y and Kekulé-O distortions. (e),(f) Schematics of the scattering in graphene with the Kekulé-Y and Kekulé-O distortions. Red, green, and blue spheres in (e) represent three groups of sites for the A sublattice and gray spheres in (e) represent the sites for the B sublattice. Red, green, and blue hexagons in (f) represent three groups of hopping parameters. (g),(h) Band structure of the $\sqrt{3} \times \sqrt{3}$ graphene lattice with Kekulé-Y and Kekulé-O distortions.

of atom A and atom B in the $(0, 0)$ unit cell. $|A_{\mathbf{R}}\rangle$ and $|B_{\mathbf{R}}\rangle$ are the p_z orbitals of carbon atoms in $\mathbf{r}_B = -\mathbf{c}$, and $|A_{\mathbf{R}}\rangle$ ($|A_{m,n}\rangle$) and $|B_{\mathbf{R}}\rangle$ ($|B_{m,n}\rangle$) are the carbon p_z orbitals on the A and B atoms in the (m, n)th unit cell. Then, the perturbation theory is introduced to explore the different effects of the Kekulé-Y and Kekulé-O distortions on the modulation of the Dirac cone of graphene. With the perturbation, the on-site energy and hopping parameter can be written as $\varepsilon_l^{m,n} = \varepsilon_0 + \epsilon_l^{m,n}$ ($l = A, B$) and $t_l^{m,n} = t + \tau_l^{m,n}$ ($l = 1, 2, 3$). Here, the unperturbed on-site energy ε_0 is set to be zero. In the space of four degenerate states of $|A\rangle$, $|B\rangle$, $|A'\rangle$, and $|B'\rangle$, the Hamiltonian can be written as

$$H = \begin{bmatrix} H_{AA} & H_{AB} & H_{AA'} & H_{AB'} \\ H_{AB}^* & H_{BB} & H_{BA'} & H_{BB'} \\ H_{AA'}^* & H_{BA'}^* & H_{A'A'} & H_{A'B'} \\ H_{AB'}^* & H_{BB'}^* & H_{A'B'}^* & H_{B'B'} \end{bmatrix}. \tag{6}$$

Here, the matrix elements of $H_{AA'}$, $H_{BB'}$, $H_{AA'}^*$, and $H_{BB'}^*$ describe the scattering in one sublattice and between two Dirac cones. The matrix elements of $H_{AB'}$, $H_{BA'}$, $H_{AB'}^*$, and $H_{BA'}^*$ describe the scattering between two sublattices and between two Dirac cones. If one of these matrix elements in each group is nonzero, the Dirac cone will open a gap.

The Kekulé-Y distortion is induced by one Li adsorbed on the top site of the carbon atom of graphene with the $\sqrt{3} \times \sqrt{3}$ supercell, which breaks the equivalence of one sublattice but keeps the equivalence of another sublattice. Under this condition, the scattering in one sublattice and between two Dirac cones is considered. Here, the Hamiltonian elements $H_{AA'}$ and $H_{BB'}$ can be written as

$$\begin{aligned} H_{AA'} &= \frac{1}{3}\left(\frac{3}{N}\sum_{m,s}\epsilon_A^{m,m+3s} + \frac{3}{N}\sum_{m,s}\epsilon_A^{m,m+3s+1}e^{2\pi i/3} + \frac{3}{N}\sum_{m,s}\epsilon_A^{m,m+3s-1}e^{-2\pi i/3}\right) \\ &= \frac{1}{3}\left(\bar{\epsilon}_A^r + \bar{\epsilon}_A^g e^{2\pi i/3} + \bar{\epsilon}_A^b e^{-2\pi i/3}\right), \end{aligned} \tag{7}$$

$$\begin{aligned} H_{BB'} &= \frac{1}{3}\left(\frac{3}{N}\sum_{m,s}\epsilon_B^{m,m+3s} + \frac{3}{N}\sum_{m,s}\epsilon_B^{m,m+3s+1}e^{2\pi i/3} + \frac{3}{N}\sum_{m,s}\epsilon_B^{m,m+3s-1}e^{-2\pi i/3}\right) \\ &= \frac{1}{3}\left(\bar{\epsilon}_B^r + \bar{\epsilon}_B^g e^{2\pi i/3} + \bar{\epsilon}_B^b e^{-2\pi i/3}\right). \end{aligned} \tag{8}$$

The $H_{AA'}$ and $H_{BB'}$ equal to zero only if $\overline{\epsilon_A^r} = \overline{\epsilon_A^g} = \overline{\epsilon_A^b}$ and $\overline{\epsilon_B^r} = \overline{\epsilon_B^g} = \overline{\epsilon_B^b}$. As shown in Fig. 5(e), the Kekulé-Y distortion can break the equivalence of one sublattice like A, but maintain the equivalence of sublattice B ($\overline{\epsilon_B^r} = \overline{\epsilon_B^g} = \overline{\epsilon_B^b}$). Therefore, the $H_{AA'}$ is nonzero, while $H_{BB'}$ is zero, indicating that the degeneracy of $|A\rangle$ and $|A'\rangle$ is broken but the degeneracy of $|B\rangle$ and $|B'\rangle$ is kept. This is the reason why the band splitting of Dirac cones can be observed in graphene with the Kekulé-Y distortion in Fig. 5(g). The Kekulé-O distortion is induced by one Li adsorbed on the hollow site of graphene with the $\sqrt{3} \times \sqrt{3}$ supercell, which breaks the equivalence of three hopping parameters. Under this condition, the scattering between two sublattices and between two Dirac cones is considered. Here, the Hamiltonian elements $H_{AB'}$ and $H_{BA'}$ can be written as

$$\begin{aligned} H_{AB'} &= \frac{1}{N}\sum_{m,n} e^{(2\pi i/3)}(m-n)\left(t_1^{m-1,n} + t_2^{m,n-1}e^{2\pi i/3} + t_3^{m,n}e^{-2\pi i/3}\right) = \frac{1}{N}\sum_{m,s}\left[t_1^{m,m+3s+1} + t_2^{m,m+3s} + t_3^{m,m+3s-1}\right] \\ &\quad + \frac{1}{N}\sum_{m,s} e^{2\pi i/3}\left[t_1^{m,m+3s} + t_2^{m,m+3s-1} + t_3^{m,m+3s+1}\right] + \frac{1}{N}\sum_{m,s} e^{-2\pi i/3}\left[t_1^{m,m+3s-1} + t_2^{m,m+3s+1} + t_3^{m,m+3s}\right] \\ &= \bar{t^r} + \bar{t^g}e^{2\pi i/3} + \bar{t^b}e^{-2\pi i/3}, \end{aligned} \tag{9}$$

$$\begin{aligned} H_{BA'} &= \frac{1}{N}\sum_{m,n} e^{2\pi i/3(m-n)}\left(t_1^{m,n} + t_2^{m,n}e^{2\pi i/3} + t_3^{m,n}e^{-2\pi i/3}\right) = \frac{1}{N}\sum_{m,s}\left[t_1^{m,m+3s} + t_2^{m,m+3s-1} + t_3^{m,m+3s+1}\right] \\ &\quad + \frac{1}{N}\sum_{m,s} e^{2\pi i/3}\left[t_1^{m,m+3s-1} + t_2^{m,m+3s+1} + t_3^{m,m+3s}\right] + \frac{1}{N}\sum_{m,s} e^{-2\pi i/3}\left[t_1^{m,m+3s+1} + t_2^{m,m+3s} + t_3^{m,m+3s-1}\right] \\ &= \bar{t^g} + \bar{t^b}e^{2\pi i/3} + \bar{t^r}e^{-2\pi i/3}. \end{aligned} \tag{10}$$

The $H_{AB'}$ and $H_{BA'}$ equal to zero only if $\overline{t^r} = \overline{t^g} = \overline{t^b}$. As shown in Fig. 5(f), the Kekulé-O distortion can break the equivalence of three hopping parameters, so the $H_{AB'}$ and $H_{BA'}$ are both nonzero, indicating that the degeneracy of $|A\rangle$ and $|B'\rangle$ and the degeneracy of $|B\rangle$ and $|A'\rangle$ are broken simultaneously. Therefore, the gap opening of Dirac cones can be observed in graphene with the Kekulé-O distortion in Fig. 5(h). All these analyses can be confirmed by the results of tight-binding calculation (shown in Fig. S6 [40]).

Li-intercalated BLG can be used as the platform for investigating the modulation of the Dirac cone since both Kekulé-Y and Kekulé-O distortion can be realized simultaneously. During the intercalation of Li, the stacking order of BLG transforms from AB to AA, accompanied by the transformation from one degenerate Dirac cone to two degenerate Dirac cones for the band structure. Two novel phenomena about the band structure of Li-intercalated BLG could be observed in the experiment. One is the band splitting of the electron pocket of the Dirac cone contributed by the Kekulé-Y distortion for $Li_{0.083}C_{12}$ (6×6, AB). Another is the gap opening of two Dirac cones contributed by the Kekulé-O distortion for LiC_{12} ($\sqrt{3} \times \sqrt{3}$, AA). The uniformly hexagonal-ordered Li might not be observed in the Li-intercalated AB-stacking BLG with the dilute concentration of Li due to the weak Coulomb repulsion of Li. However, the Friedel oscillation would induce the hidden Kekulé order that the splitting of the electron pocket of the Dirac cone could be observed in the generalized Kekulé patterned BLG with AB stacking order, such as $Li_{0.083}C_{12}$ (6×6, AB) [13,15]. Once the BLG is intercalated with the high concentration of Li, the highly ordered hexagonal distribution of Li could be observed due to the strong Coulomb repulsion of Li [38,39], as well as the stacking order transformation from AB to AA. Under this condition, the repetitive gap opening of two Dirac cones of AA-stacking BLG could be observed by the *in situ* ARPES measurement because of the successive formation of $Li_{0.25}C_{12}$ ($2\sqrt{3} \times 2\sqrt{3}$, AA), $Li_{0.333}C_{12}$ (3×3, AA), and LiC_{12} ($\sqrt{3} \times \sqrt{3}$, AA) superlattices with the generalized Kekulé order during the intercalation of Li.

IV. CONCLUSIONS

Besides Bernal stacking BLG (1×1, AB) and LiC_{12} ($\sqrt{3} \times \sqrt{3}$, AA), four stable Li-intercalated BLG structures of $Li_{0.083}C_{12}$ (6×6, AB), $Li_{0.188}C_{12}$ (4×4, AA), $Li_{0.231}C_{12}$ ($\sqrt{13} \times \sqrt{13}$, AA), and $Li_{0.75}C_{12}$ (2×2, AA) can serve as a landmark for the experiment to study the intercalation of Li into BLG. Moreover, the observation of the generalized Kekulé order and the different effects of the Kekulé-Y and Kekulé-O distortions on the Dirac cone of graphene, as well as the exploration of their origins, provide a further understanding of Li-intercalated BLG, which can be used for exploring other related physics.

ACKNOWLEDGMENTS

This work was supported by the National Key R&D Program of China (Grant No. 2021YFA1400100), the National Natural Science Foundation of China (Grants No. 12274254 and No. 11874036), Local Innovative and Research Teams Project of Guangdong Pearl River Talents Program (Grant No. 2017BT01N111), Science and Technology Planning Project of Guangdong Province (Grant No. 2020B1212060015), and Shenzhen Basic Research Project (No. JCYJ20200109142816479).

[1] V. N. Kotov, B. Uchoa, V. M. Pereira, F. Guinea, and A. H. Castro Neto, Rev. Mod. Phys. **84**, 1067 (2012).

[2] A. H. Castro Neto, F. Guinea, N. M. R. Peres, K. S. Novoselov, and A. K. Geim, Rev. Mod. Phys. **81**, 109 (2009).

[3] C. L. Kane and E. J. Mele, Phys. Rev. Lett. **95**, 226801 (2005).

[4] S. Y. Zhou, G. H. Gweon, A. V. Fedorov, P. N. First, W. A. de Heer, D. H. Lee, F. Guinea, A. H. Castro Neto, and A. Lanzara, Nat. Mater. **6**, 770 (2007).

[5] C. H. Lui, Z. Li, K. F. Mak, E. Cappelluti, and T. F. Heinz, Nat. Phys. **7**, 944 (2011).

[6] E. V. Castro, K. S. Novoselov, S. V. Morozov, N. M. R. Peres, J. M. B. Lopes dos Santos, J. Nilsson, F. Guinea, A. K. Geim, and A. H. Castro Neto, Phys. Rev. Lett. **99**, 216802 (2007).

[7] Z. Lin, W. Qin, J. Zeng, W. Chen, P. Cui, J. H. Cho, Z. Qiao, and Z. Zhang, Nano Lett. **17**, 4013 (2017).

[8] S. H. Lee, H. J. Chung, J. Heo, H. Yang, J. Shin, U. I. Chung, and S. Seo, ACS Nano **5**, 2964 (2011).

[9] J. L. Mañes, F. Guinea, and M. A. H. Vozmediano, Phys. Rev. B **75**, 155424 (2007).

[10] T. Ohta, A. Bostwick, T. Seyller, K. Horn, and E. Rotenberg, Science **313**, 951 (2006).

[11] K. K. Gomes, W. Mar, W. Ko, F. Guinea, and H. C. Manoharan, Nature (London) **483**, 306 (2012).

[12] M. Farjam and H. Rafii-Tabar, Phys. Rev. B **79**, 045417 (2009).

[13] V. V. Cheianov, V. I. Fal'ko, O. Syljuåsen, and B. L. Altshuler, Solid State Commun. **149**, 1499 (2009).

[14] D. Ma, Z. Fu, X. Sui, K. Bai, J. Qiao, C. Yan, Y. Zhang, J. Hu, Q. Xiao, X. Mao, W. Duan, and L. He, ACS Nano **12**, 10984 (2018).

[15] C. Gutiérrez, C.-J. Kim, L. Brown, T. Schiros, D. Nordlund, E. Lochocki, K. M. Shen, J. Park, and A. N. Pasupathy, Nat. Phys. **12**, 950 (2016).

[16] N. M. Caffrey, L. I. Johansson, C. Xia, R. Armiento, I. A. Abrikosov, and C. Jacobi, Phys. Rev. B **93**, 195421 (2016).

[17] M. Calandra and F. Mauri, Phys. Rev. Lett. **95**, 237002 (2005).

[18] J. Xu, Y. Dou, Z. Wei, J. Ma, Y. Deng, Y. Li, H. Liu, and S. Dou, Adv. Sci. (Weinheim, Ger.) **4**, 1700146 (2017).

[19] Y. Li, Y. Lu, P. Adelhelm, M.-M. Titirici, and Y.-S. Hu, Chem. Soc. Rev. **48**, 4655 (2019).

[20] H. Kim, J. C. Kim, M. Bianchini, D.-H. Seo, J. Rodriguez-Garcia, and G. Ceder, Adv. Energy Mater. **8**, 1702384 (2017).

[21] E. Lee and K. A. Persson, Nano Lett. **12**, 4624 (2012).

[22] K. Persson, Y. Hinuma, Y. S. Meng, A. Van der Ven, and G. Ceder, Phys. Rev. B **82**, 125416 (2010).

[23] J. Liu, T. Yin, B. Tian, B. Zhang, C. Qian, Z. Wang, L. Zhang, P. Liang, Z. Chen, J. Yan, X. Fan, J. Lin, X. Chen, Y. Huang, K. P. Loh, and Z. X. Shen, Adv. Energy Mater. **9**, 1900579 (2019).

[24] J. Zhao, X. Zou, Y. Zhu, Y. Xu, and C. Wang, Adv. Funct. Mater. **26**, 8103 (2016).

[25] N. Ehlen, M. Hell, G. Marini, E. H. Hasdeo, R. Saito, Y. Falke, M. O. Goerbig, G. Di Santo, L. Petaccia, G. Profeta, and A. Grüneis, ACS Nano **14**, 1055 (2020).

[26] G. Profeta, M. Calandra, and F. Mauri, Nat. Phys. **8**, 131 (2012).

[27] E. Andrade, R. Carrillo-Bastos, and G. G. Naumis, Phys. Rev. B **99**, 035411 (2019).

[28] J. J. Wang, S. Liu, J. Wang, and J.-F. Liu, Phys. Rev. B **98**, 195436 (2018).

[29] O. V. Gamayun, V. P. Ostroukh, N. V. Gnezdilov, İ. Adagideli, and C. W. J. Beenakker, New J. Phys. **20**, 023016 (2018).

[30] K. Sugawara, K. Kanetani, T. Sato, and T. Takahashi, AIP Adv. **1**, 022103 (2011).

[31] C. Bao, H. Zhang, T. Zhang, X. Wu, L. Luo, S. Zhou, Q. Li, Y. Hou, W. Yao, L. Liu, P. Yu, J. Li, W. Duan, H. Yao, Y. Wang, and S. Zhou, Phys. Rev. Lett. **126**, 206804 (2021).

[32] G. Kresse and J. Furthmüller, Phys. Rev. B **54**, 11169 (1996).

[33] G. Kresse and D. Joubert, Phys. Rev. B **59**, 1758 (1999).

[34] P. E. Blöchl, Phys. Rev. B **50**, 17953 (1994).

[35] J. P. Perdew, K. Burke, and M. Ernzerhof, Phys. Rev. Lett. **77**, 3865 (1996).

[36] S. Grimme, S. Ehrlich, and L. Goerigk, J. Comput. Chem. **32**, 1456 (2011).

[37] V. Popescu and A. Zunger, Phys. Rev. B **85**, 085201 (2012).

[38] K. Ji, J. Han, A. Hirata, T. Fujita, Y. Shen, S. Ning, P. Liu, H. Kashani, Y. Tian, Y. Ito, J. I. Fujita, and Y. Oyama, Nat. Commun. **10**, 275 (2019).

[39] C.-L. Song, B. Sun, Y.-L. Wang, Y.-P. Jiang, L. Wang, K. He, X. Chen, P. Zhang, X.-C. Ma, and Q.-K. Xue, Phys. Rev. Lett. **108**, 156803 (2012).

[40] See Supplemental Material at http://link.aps.org/supplemental/10.1103/PhysRevB.107.165409 for additional information to the main text.